HHS Public Access

Author manuscript

Nat Metab. Author manuscript; available in PMC 2019 November 01.

Published in final edited form as:

Nat Metab. 2019 May ; 1(5): 519–531. doi:10.1038/s42255-019-0063-6.

Nrf2 controls iron homeostasis in haemochromatosis and thalassaemia via Bmp6 and hepcidin

Pei Jin Lim[1], **Tiago L. Duarte**[2], **João Arezes**[1], **Daniel Garcia-Santos**[3,4,¶], **Amel Hamdi**[3,4,¶], **Sant-Rayn Pasricha**[1,5], **Andrew E. Armitage**[1], **Hema Mehta**[6], **Sarah Wideman**[1], **Ana G. Santos**[2], **Andreia Santos-Gonçalves**[2], **Alireza Morovat**[7], **Jim R. Hughes**[8], **Elizabeth Soilleux**[9], **Chia-Yu Wang**[10], **Abraham L. Bayer**[10], **Paul Klenerman**[5,11], **Christian B. Willberg**[5], **Richard C. Hartley**[12], **Michael P. Murphy**[13], **Jodie L. Babitt**[10], **Prem Ponka**[3,4], **Graça Porto**[2], and **Hal Drakesmith**[1,14]

[1]MRC Human Immunology Unit, MRC Weatherall Institute of Molecular Medicine, University of Oxford, John Radcliffe Hospital, Oxford, OX3 9DS, UK

[2]Instituto de Biologia Molecular e Celular & Instituto de Investigação e Inovação em Saúde, Universidade do Porto, Porto, Portugal

[3]Lady Davis Institute for Medical Research, Jewish General Hospital, Montreal, QC, Canada

[4]Department of Physiology, McGill University, Montreal, QC, Canada

[5]The Walter and Eliza Hall Institute of Medical Research, Parkville, Australia

[6]Peter Medawar Building for Pathogen Research, University of Oxford, Oxford, Oxfordshire, UK

[7]Department of Clinical Biochemistry, Oxford University Hospitals NHS Foundation Trust, UK

[8]MRC Molecular Haematology Unit, MRC Weatherall Institute of Molecular Medicine. University of Oxford, John Radcliffe Hospital, Oxford, OX3 9DS, UK

[9]Department of Cellular Pathology, Oxford University Hospitals NHS Trust, John Radcliffe Hospital, Oxford, UK

[10]Nephrology Division, Program in Membrane Biology, Center for Systems Biology, Massachusetts General Hospital and Harvard Medical School, Boston, Massachusetts, USA

Correspondence to: Hal Drakesmith, MRC Human Immunology Unit, MRC Weatherall Institute of Molecular Medicine, University of Oxford, John Radcliffe Hospital, Oxford, OX3 9DS, UK., alexander.drakesmith@imm.ox.ac.uk, Telephone: +44(0)1865 222699, Fax: +44(0)1865 222406.

¶These authors contributed equally

Author Contributions

Designed research: PJL, TLD, CBW, DGS, PP, AEA, SRP, HD

Collected data: PJL, TLD, AEA, JA, HM, DGS, AH, SW, SRP, JRH, AGS, ALB, ASG, AM, ES, CYW, JLB

Analyzed and interpreted data: PJL, HD, TLD, DGS, PP, PK, AEA, SRP, ES, RCH, MPM, CYW, JLB, GP

Wrote the manuscript: PJL, HD

Competing financial interests

The authors declare no competing financial interests.

Reporting summary

Further information on experimental design is available in the Reporting Summary.

Data availability statement

The datasets generated during and/or analysed during the current study are available from the corresponding author on reasonable request.

[11]Oxford NIHR Biomedical Research Centre, The John Radcliffe Hospital, Oxford, UK

[12]WestCHEM School of Chemistry, University of Glasgow, Glasgow, G12 8QQ, UK

[13]MRC Mitochondrial Biology Unit, University of Cambridge, Cambridge, CB2 0XY, UK

[14]Haematology Theme Oxford Biomedical Research Centre, Oxford, UK

Abstract

Iron is critical for life but toxic in excess because of iron-catalysed formation of pro-oxidants that cause tissue damage in a range of disorders. The Nrf2 transcription factor orchestrates cell-intrinsic protective antioxidant responses, and the peptide hormone hepcidin maintains systemic iron homeostasis, but is pathophysiologically decreased in haemochromatosis and beta-thalassaemia. Here, we show that Nrf2 is activated by iron-induced, mitochondria-derived pro-oxidants and drives Bmp6 expression in liver sinusoid endothelial cells, which in turn increases hepcidin synthesis by neighbouring hepatocytes. In Nrf2 knockout mice, the Bmp6-hepcidin response to oral and parenteral iron is impaired and iron accumulation and hepatic damage are increased. Pharmacological activation of Nrf2 stimulates the Bmp6-hepcidin axis, improving iron homeostasis in haemochromatosis and counteracting the inhibition of Bmp6 by erythroferrone in beta-thalassaemia. We propose that Nrf2 links cellular sensing of excess toxic iron to control of systemic iron homeostasis and antioxidant responses, and may be a therapeutic target for iron-associated disorders.

Iron facilitates the oxygen-carrying capacity of blood and serves as a critical component for many cellular processes including DNA replication and energy transduction[1]. Defects in iron balance contribute to the pathogenesis of cancer, diabetes, cardiovascular disease, metabolic syndrome, as well as haemochromatosis, thalassaemia and anaemia. Oral and parenteral iron treatments are amongst the most commonly administered medical interventions worldwide. The amount and distribution of iron is regulated systemically by the liver-expressed hormone hepcidin (encoded by *Hamp1*)[2]. Hepcidin induces the degradation of the iron exporter ferroportin[3], limiting dietary iron absorption by enterocytes and iron recycling from senescent erythrocytes by macrophages. Appropriate regulation of hepcidin synthesis in response to fluctuating iron levels is critical to maintain iron homeostasis. Hepcidin deficiency causes pathological iron overload in the common genetic disorders hereditary haemochromatosis[4] and beta-thalassaemia[5]. Hepcidin regulation in response to iron is controlled by BMP/SMAD signalling and by *Bmp6* expression[6]. *Bmp6*-deficient mice have very low hepcidin levels and accrue severe iron accumulation[7,8]. Liver sinusoidal endothelial cells (LSECs) are the predominant source of hepatic Bmp6[9]. The intracellular mechanism by which iron is sensed and converted into a signal to regulate hepatic *Bmp6* expression is not known.

Excess iron, resulting from iron overload disorders, or because of oral or parenteral iron treatments, induces oxidative stress[10,11]. By responding to toxic insults and controlling the expression of detoxification and antioxidant enzymes, the transcription factor Nrf2 maintains cellular health in the face of intracellular and environmental stresses[12], and so is a key player in carcinogenesis. At basal conditions, Nrf2 is sequestered in the cytoplasm by Keap1

(Kelch-like ECH-associated protein 1), an adaptor subunit of Cullin3 E3 ubiquitin ligase, and targeted for ubiquitination and degradation. Oxidative stress-inducing stimuli destabilize the Nrf2-Keap1-Cullin3 complex and block Nrf2 degradation. This allows *de novo* synthesized Nrf2 to translocate into the nucleus, bind antioxidant response elements (AREs), and control the expression of genes encoding proteins with antioxidant and cytoprotective properties, such as NAD(P)H dehydrogenase quinone 1 (*Nqo1*) and Glutamate-Cysteine Ligase Catalytic Subunit (*Gclc)*[12,13]. The Bach1 (Btb and Cnc Homology 1) transcriptional repressor negatively controls the expression of ARE-regulated genes, including heme oxygenase 1 (*Hmox1*) [14].

Here we show that induction of *Bmp6* expression is regulated by the Nrf2-Keap1-Bach1 system in response to iron-induced mitochondrial reactive lipid species and heme. Nrf2 deficiency impairs control of hepcidin in the context of iron supplementation and associates with iron toxicity, while Nrf2 activation stimulates the Bmp6-hepcidin axis and enhances antioxidant defences. Therefore Nrf2 has systemic in addition to cell-intrinsic detoxifying properties that have relevance to a range of disorders in which iron accumulation is pathogenic.

Results

Iron activates Nrf2 and Bmp6 is regulated by Nrf2

Hepatic *Bmp6* is upregulated by iron in mice[6] and in hereditary hemochromatosis[15,16]. In separate studies, elevated hepatic iron content in mice fed high-iron diets was associated with increased Nrf2 activity[17,18]. We tested whether concurrent Nrf2 activation and *Bmp6* upregulation was generalizable across several models of iron overload. We investigated how altering iron *in vivo* affected hepatic expression of *Bmp6*, downstream Bmp/Smad-target genes (*Hamp1*, *Id1*, *Smad7*) and Nrf2-target genes (*Nqo1*, *Hmox1*, *Gclc*). Mice fed high iron diet (1% carbonyl iron) for 3 weeks had increased liver iron content as well as raised *Bmp6, Hamp1, Id1* and *Smad7* gene expression, coupled with upregulation of *Nqo1*, *Hmox1* and *Gclc* consistent with Nrf2 activation (Fig. 1a). Intraperitoneal administration of 4mg FeDx increased liver iron content 6 hours later, with concomitant upregulation of hepatic *Bmp6*, *Nqo1*, *Hmox1*, *Gclc, Hamp1* and *Id1* mRNA expression (Supplementary Fig. 1a). The concurrent induction of these six mRNAs was dose-dependent over 24 hours and was observed in male and female mice (Supplementary Fig. 1b, c). To cause iron accumulation by genetic intervention, we deleted hepcidin in a previously described inducible *Hamp1*-knockout (i*Hamp1*-KO) model[19]. Tamoxifen-treated i*Hamp1*-KO mice were hepcidin-deficient, accumulated liver iron and had increased *Bmp6, Id1* and *Smad7* expression, concomitant with upregulation of *Nqo1*, *Hmox1* and *Gclc* expression (Supplementary Fig. 1d). Concurrent upregulation of *Bmp6* together with *Nqo1*, *Hmox1* and *Gclc* was also observed in LSECs purified *ex vivo* following *in vivo* iron loading in 129S6/SvEvTac mice fed 1% carbonyl iron (high) versus 37ppm iron (low) diets for 4 weeks (Fig. 1b). *In vitro*, ferric ammonium citrate (FAC) increased *Bmp6*, *Nqo1*, *Hmox1* and *Gclc* expression in primary murine LSECs (Fig. 1c), C2C12 cells and MEF cells and upregulated *BMP6* in the human LSEC-derived cell-line TMNK-1 (Supplementary Fig. 1e). In L929 cells FeDx

upregulated *Bmp6*, concurrently led to nuclear accumulation of Nrf2 and increased expression of *Nqo1*, *Hmox1* and *Gclc* (Fig. 1d).

Since concurrent upregulation of Nrf2 target genes and *Bmp6* was observed across several *in vitro* and *in vivo* models of iron loading, we hypothesized that *Bmp6* could be regulated by the Nrf2/Keap1/Bach1 system. Publicly available ChIP-seq data showed Nrf2 binds in intron 1 of the murine *Bmp6* locus in C2C12 cells treated with an agonist of Nrf2 (CDDO-Im[20–22]) and this binding site overlaps with an Nrf2 ChIP peak in *Keap1*−/− MEF cells (Fig. 1e). The ChIP-seq peak overlaps with an H3K4-monomethylation (H3K4me1) enhancer mark and RNA polymerase II binding region in MEF cells, is highly conserved in mammals, and contains an ARE consensus sequence TGCTGAGTCA[23] (Fig. 1e). Nrf2 ChIP-seq peaks were also observed at well-characterised and similarly conserved AREs with the same TGCTGAGTCA consensus sequence in the *Hmox1* and *Nqo1* promoters[24] in both Nrf2 ChIP-seq datasets analysed (Supplementary Fig. 2a,b). To test whether baseline *Bmp6* expression was sensitive to changes in *Nrf2*, *Keap1* and *Bach1*, we knocked down expression of these three genes in C2C12, MEF and L929 cells. In C2C12 cells (Fig. 1f–h), knockdown of Nrf2 led to a decrease of *Bmp6* expression, whereas knockdown of Keap1 (which targets Nrf2 for degradation) or Bach1 (which generally suppresses Nrf2 target genes) led to an increase in *Bmp6* expression; similar effects were observed on expression of Nrf2 target genes *Nqo1* and *Gclc*, while *Hmox1* expression was not altered by *Nrf2* or *Keap1* knockdown but strongly upregulated by *Bach1* knockdown as expected[24]. Similar effects of *Nrf2, Keap1* and *Bach1* knockdown on expression of *Bmp6* and other Nrf2 target genes were observed in L929 and MEF cells (Supplementary Fig. 1f–k). The suppressive activity of Bach1 can be counteracted by heme[14], which induces Bach1 degradation; we found that hemin (heme chloride) induced loss of whole cell and nuclear Bach1 protein, caused nuclear accumulation of Nrf2, and increased expression of *Bmp6* and other Nrf2 target genes in L929 cells (Supplementary Fig. 3a). In livers of mice injected with hemin, *Bmp6, Nqo1, Gclc* and *Hmox1* expression was also increased (Supplementary Fig. 3b). In summary, the *Bmp6* locus is bound by Nrf2 at a conserved ARE site, experimental manipulation of endogenous Nrf2 activity by siRNA alters expression of *Bmp6* and other Nrf2-regulated genes, and iron treatments that activate Nrf2 increase expression of *Bmp6* alongside canonical Nrf2 target genes.

Iron-induced mitochondria-derived pro-oxidants activate Nrf2

We further investigated how iron activates Nrf2 and induces *Bmp6* expression. Inflammation caused by LPS can activate Nrf2 in macrophages via induction of Irg1 expression, leading to production of itaconate, which alkylates Keap1[25]. However, *Irg1* mRNA was not detected after 40 cycles of quantitative RT-PCR in L929 or C2C12 cells at baseline or after iron treatment, and hepatic *Irg1* was not altered in mice injected with FeDx (in which mRNA levels of inflammatory genes *Fga1* and *Saa1* were also unaltered) or subjected to a high-iron diet for one week (in which *Fga1* was upregulated but *Saa1* was not altered) (Supplementary Fig. 4a, b). Therefore Irg1/itaconate is highly unlikely to be involved in regulation of *Bmp6* by iron and Nrf2. Instead we hypothesized that Nrf2 activation by iron could occur via the generation of ROS. By quantifying the lipid peroxidation product malondialdehyde (MDA) in liver lysates, we found that C57BL/6 mice fed a week of high iron diet experienced more

hepatic lipid peroxidation than mice on a control iron diet (Fig. 2a). The mitochondrial electron transport chain is a major source of cellular ROS, and excess iron may promote mitochondrial ROS, oxidative damage and lipid peroxidation[26,27]. To assess how the generation of ROS influences *Bmp6* induction by iron, we used the free radical scavenger mitoTEMPO[28], which concentrates in the mitochondria matrix and acts to quench ROS and oxidative damage (Fig. 2b). In L929 cells, mitoTEMPO prevented upregulation of *Bmp6* by FeDx, blunted *Nqo1* upregulation but did not alter upregulation of *Hmox1* (Fig. 2c). FeDx treatment increased the ratio of Nrf2:lamin A in the nucleus of L929 cells by >70%, but in the presence of mitoTEMPO, the ratio of Nrf2/lamin A was unchanged by FeDx, indicating a role for mitochondria-derived ROS production and/or oxidative damage for Nrf2 activation in response to iron (Supplementary Fig 4c). In mice, oral gavage with 2mg/kg iron did not measurably alter hepatic iron content by 6 hours but acutely raised serum iron (Fig. 2d) as well as hepatic *Nqo1, Hmox1* and *Bmp6* expression (Fig. 2e). mitoTEMPO completely blocked the induction of *Bmp6* and *Hmox1* by iron gavage, although upregulation of *Nqo1* was maintained (Fig. 2e). We then tested the effects of generating mitochondrial ROS (specifically superoxide) in the absence of added iron by using the mitochondria-targeted redox cycler MitoParaquat (MitoPQ)[29]; increased superoxide potentiates lipid peroxidation within mitochondria that leads to release of electrophilic reactive lipid species[30] (RLS) (Fig 2f). *Bmp6, Nqo1* and *Hmox1* were induced in cells treated with MitoPQ (Fig. 2g), but not by a control compound that similarly targets mitochondria but does not generate superoxide[31] (Supplementary Fig. 4d,e). Therefore selective generation of ROS within mitochondria and the associated oxidative damage that can be induced by iron are necessary and sufficient to drive expression of Nrf2 target genes, including *Bmp6*. It is the pro-oxidant activity of iron, rather than iron *per se*, that activates Nrf2 and induces *Bmp6*.

Nrf2 regulates stimulation of the Bmp6-hepcidin axis by iron

Next we asked whether Nrf2 was required for upregulation of Bmp6 by iron. Knockdown of *Nrf2* completely blocked the upregulation of *Bmp6* and *Nqo1* by FeDx in L929 (Fig. 3a), and in C2C12 cells the upregulation of *Bmp6* and *Nqo1* by FAC was blunted by knockdown of Nrf2 (Fig. 3b). *In vivo*, 24 hours after intraperitoneal injection of FeDx in $Nrf2^{-/-}$, $Nrf2^{+/-}$ and $Nrf2^{+/+}$ littermate mice, induction of hepatic *Bmp6* and *Nqo1* expression by FeDx was blunted in $Nrf2^{-/-}$ mice, with an intermediate response in heterozygotes, and importantly, *Hamp1* induction by FeDx was also significantly blunted in *Nrf2* deficient mice (Supplementary Fig. 5). This decrease in hepcidin levels led us to test the effect of Nrf2 deficiency in the context of more chronic iron accumulation (increased liver iron was a previously unexplained finding in $Nrf2^{-/-}$ mice[32]). After one week on a high iron (1% carbonyl diet), $Nrf2^{-/-}$ mice had decreased hepatic expression of *Nqo1, Gclc, Bmp6* and *Hamp1* compared to wild-type controls, and although liver iron accumulation was not different between the two groups as a whole, some $Nrf2^{-/-}$ mice had accumulated more liver iron (Fig 3c). To test this further, $Nrf2^{-/-}$ and $Nrf2^{+/+}$ littermate mice were fed control (200ppm iron) or high iron (2% carbonyl iron) diet for 2 weeks. Again, $Nrf2^{-/-}$ mice failed to upregulate hepatic *Bmp6* and had blunted *Nqo1* induction in response to hepatic iron accumulation, and furthermore the upregulation of Bmp/Smad-target genes *Id1* and *Smad7* was also abrogated (Fig. 3d). The upregulation of hepcidin by iron in $Nrf2-/-$ mice was blunted by about 25%, showing that Nrf2-controlled induction of Bmp6 makes a non-

redundant contribution to control of hepcidin in response to chronic iron overload (Fig 3e). Furthermore, in this experiment, *Nrf2*$^{-/-}$ mice had ~ 27% higher levels of hepatic iron than wild-type controls (Fig 3f), and after 4 weeks of 1% carbonyl iron diet, *Nrf2−/−* mice accumulated 30% more iron in the liver than wildtype animals (Fig. 3g). These findings could not be accounted for by differences in relative liver weight as we previously showed no difference in weight of livers between iron loaded wildtype and *Nrf2*$^{-/-}$ animals[18]. Ferroportin is an Nrf2-regulated gene[33] and we considered whether altered ferroportin expression could contribute to the iron loading phenotype. However, Nrf2 genotype did not affect hepatic ferroportin mRNA levels at baseline or 24 hours after intraperitoneal injection of FeDx; Nrf2 genotype also did not influence splenic ferroportin mRNA at baseline or after FeDx treatment, or affect splenic iron accumulation after one and four weeks of high iron diets (Supplementary Fig 6a–c). Hepatic *Slc39a14* (encoding Zip14) can also influence liver iron accumulation[34], but hepatic *Slc39a14* mRNA was not different between wild-type and *Nrf2−/−* mice either at baseline or after 2 weeks of high iron diet, and so is not obviously Nrf2-regulated (Supplementary Fig 6d). Therefore the iron loading phenotypes we observe in *Nrf2−/−* mice are unlikely to be due to altered transcriptional regulation of ferroportin or Zip14.

Nrf2 controls iron-mediated damage to hepatocytes and LSECs

Because Nrf2, as well as controlling the Bmp6-hepcidin axis, also regulates protective antioxidant effects, we analysed how Nrf2 deficiency would influence liver pathology. We observed a greater increase in lipid peroxidation (MDA) in *Nrf2*$^{-/-}$ mice after 4 weeks of dietary iron loading; hepatic expression of liver fibrosis markers collagen type 1 (*Col1a1*) and transgelin (*Tagln*) were also higher in iron-loaded *Nrf2*$^{-/-}$ mice (Fig. 4a). This suggested that as well as being disposed to over-accumulate iron, *Nrf2*$^{-/-}$ mice are also more susceptible to iron-induced liver oxidative damage and subsequent tissue injury. Consistent with this idea, when *Nrf2*$^{-/-}$ and wildtype mice were given a single intraperitoneal injection of FeDx, increased hepatic necroinflammatory foci developed over 30 days in *Nrf2*$^{-/-}$ mice (Fig. 4b,c). Previously we described ultrastructural hepatocyte pathology in iron-exposed *Nrf2*$^{-/-}$ mice[18]. Because LSECs are the key source of Bmp6[9], and because Nrf2 is required for induction of Bmp6 by iron, we further examined ultrastructural features of LSECs in iron-loaded wild-type and *Nrf2*$^{-/-}$ mice. In liver sinusoids of wild-type animals fed 2% carbonyl iron diet for two weeks, cristae of LSEC mitochondria were well-formed, as were hepatocyte mitochondria, and hepatocyte microvilli in the space of Disse were evident (Fig 4d). In contrast, in iron-loaded *Nrf2*$^{-/-}$ mice, mitochondrial injuries were apparent in both LSECs and hepatocytes, including swelling and loss of cristae or matrix, microvilli were decreased, and some deposition of collagen fibres was observed (Fig 4e,f). In iron loaded *Nrf2*$^{-/-}$ mice also treated daily with mitoTEMPO, a rescue of the phenotype occurred, with better preserved LSEC and hepatocyte mitochondria, and microvilli of the hepatocytes extending into the space of Disse (Fig 4g,h). Together these data show that Nrf2 is required for sensing and protecting against iron-induced mitochondrial ROS production and oxidative damage, and that the absence of Nrf2 in the context of iron loading leads to both defective hepcidin regulation and tissue damage.

Nrf2 controls serum iron levels in *Hfe* deficient mice

To build on these observations, we investigated the role of Nrf2 in hereditary hemochromatosis (HH). In humans the commonest form of HH is caused by mutations in *HFE*, but while *Hfe*−/− mice model the iron overload of the human disease, they do not recapitulate several other aspects of pathology, including liver fibrosis[35]. Hfe/Nrf2 double knockout (*Hfe*/*Nrf2*$^{-/-}$) mice on standard diet showed signs of increased liver damage and fibrosis over time, indicating that *Nrf2* deficiency modifies disease progression[36]. We measured hepatic *Bmp6* expression at six-month intervals over two years in wildtype, *Nrf2*−/−, *Hfe*−/− and *Hfe*/*Nrf2*$^{-/-}$ mice and analysed the data by 2-way ANOVA, stratifying on age of mice, to look at the effects of genotype on iron and hepatic gene expression. *Bmp6* was higher in *Hfe*−/− mice compared with wildtypes, likely as a result of iron accumulation[15]; however Nrf2 deficiency caused a decrease in *Bmp6* expression even in *Hfe*−/− mice (Supplementary Fig. 7a). *Nrf2* deficiency (against a wild-type or *Hfe*−/− background) also decreased *Nqo1* expression (Supplementary Fig. 7b). *Hamp1* levels were decreased in *Nrf2*−/−, *Hfe*−/− and *Hfe*/*Nrf2*$^{-/-}$ mice, and liver iron was increased in *Hfe*−/− and *Hfe*/*Nrf2*$^{-/-}$ mice (Supplementary Fig. 7c,d). We noted a tendency for the lowest *Hamp1* mRNA and highest liver iron accumulation to occur in the oldest *Hfe*/*Nrf2*$^{-/-}$ animals, and this prompted us to investigate iron loading in other organs affected in HH. We observed significant iron accumulation and stainable iron deposits in the heart and pancreas of 24-month old *Hfe*/*Nrf2*$^{-/-}$ mice (Supplementary Fig. 7e). Together with our previous findings[36] these data indicate that in the context of murine HH, loss of Nrf2 leads to increased parenchymal iron deposition and increased iron-associated tissue damage.

These findings led us to hypothesize that pharmacological activation of Nrf2, achieved using the small molecule CDDO-Im that activates Nrf2 via destabilising the Nrf2/Keap1 interaction[21], would improve the phenotype of *Hfe*$^{-/-}$ mice. First, we established that after 6 hours, CDDO-Im increased *Bmp6* and *Hmox1* expression in primary murine LSECs and the human LSEC line TMNK-1 (Fig 5a), and in wild-type but not *Nrf2*−/− murine livers (Fig. 5b). LSECs are also the source of *Bmp2*, which contributes to hepatic hepcidin regulation[37], however CDDO-Im did not influence LSEC *Bmp2* expression and had only very small effects on hepatic *Bmp2* expression *in vivo* (Fig 5a,b). To test the effects of Nrf2 activation in the context of hemochromatosis, we next gave *Hfe*−/− mice 30μmol/kg CDDO-Im for 6 hours. Compared to vehicle-treated *Hfe*−/− mice, CDDO-Im increased hepatic expression of *Nqo1, Bmp6* (but not *Bmp2*), *Hamp1*, and decreased serum iron (Fig 5c). Hepcidin is unlikely to be directly regulated by CDDO-Im, because in mice expressing a constitutively active form of Nrf2 in hepatocytes, in which hepatic expression of canonical Nrf2 target genes are strongly upregulated[38], liver *Hamp1* expression is unchanged (Kohler UA and Werner S, personal communication). Nevertheless a requirement for *Hamp1* for CDDO-Im mediated decrease of serum iron was confirmed by treatment of *Hamp1*$^{-/-}$ mice with CDDO-Im for 6 hours; CDDO-Im increased *Bmp6* (but not *Bmp2*), *Nqo1, Gclc* and *Hmox1* mRNA, but serum iron was not decreased (Supplementary Fig. 8a,b). As a further control, we tested *Bmp6fl/fl;Tek-Cre*+ mice that lack *Bmp6* in LSECs, which are iron-loaded due to insufficient hepcidin expression[9]. CDDO-Im treatment of these mice increased hepatic expression of the canonical Nrf2 target gene *Nqo1*, but did not increase hepatic *Bmp6*, or

Hamp1, or decrease serum iron levels (Supplementary Fig. 8c,d). Thus, in iron-loaded mice, Nrf2 activation decreases serum iron in a manner that requires LSEC *Bmp6* and hepcidin.

Activation of Nrf2 inhibits iron loading in haemochromatosis

To the test the effects of chronic Nrf2 activation on organ iron accumulation, we gave 8-week old female *Hfe*$^{-/-}$ mice 10 doses of 30μmol/kg CDDO-Im over 3 weeks. At the end of treatment, mice given CDDO-Im had increased Nrf2 protein in livers and upregulated hepatic *Bmp6* (with *Bmp2* unchanged), *Nqo1* and *Hmox1* expression, showing ongoing Nrf2 activation (Fig. 5d). *Hfe*$^{-/-}$ mice given CDDO-Im accumulated three-fold less hepatic iron than vehicle-treated *Hfe*$^{-/-}$ mice over the three-week treatment (Fig. 5e). Indeed, CDDO-Im exposed mice did not appear to accumulate liver iron over the three week treatment period as their liver iron levels at 11 weeks of age were not significantly different from 8 week old *Hfe−/−* mice ('NS' in Fig 5e). CDDO-Im also decreased serum iron relative to vehicle-treated controls, and splenic iron was marginally although non-significantly reduced (Fig 5e). Together, these results indicate a decrease in systemic iron loading. The reduction in liver iron content was evident by Perls' staining, which showed less iron in CDDO-Im-treated mice (Fig. 5f). Despite the lower hepatic and serum iron, which normally decrease hepcidin expression, hepcidin mRNA and serum hepcidin protein were similar in CDDO-Im treated mice at the end of the treatment period, so that higher serum hepcidin to serum iron ratios were apparent in mice given CDDO-Im (Fig. 5g). We also noted decreased liver lipid peroxidation, a marker of oxidative damage, in CDDO-Im treated *Hfe−/−* mice (Fig 5h). Consistent with the data on acute (6hour) Nrf2 activation on iron, a role for hepcidin in the decreased iron accumulation due to CDDO-Im was supported by experiments with *Hamp1*$^{-/-}$ mice treated with CDDO-Im over 3 weeks. Unlike *Hfe−/−* mice and despite increased hepatic expression of *Bmp6* and other Nrf2 target genes, CDDO-Im treated *Hamp1*$^{-/-}$ mice did not have decreased hepatic iron accumulation or serum iron compared to vehicle-treated mice (Supplementary Fig. 8e,f). Thus the inhibition of systemic iron accumulation by CDDO-Im in *Hfe*−/− mice is mediated by upregulation of the *Bmp6*-hepcidin axis, increasing the hepcidin:iron ratio over time and alleviating iron overload and hepatic oxidative damage.

Nrf2 counteracts suppression of hepcidin in thalassaemia

Toxic iron accumulation also occurs in non-transfusion-dependent thalassaemia, caused at least in part by chronic EPO-induced erythroblast expression of erythroferrone, which suppresses hepcidin synthesis[39]. Erythroferrone inhibits the induction of hepcidin by blocking Bmp6[40], so we hypothesised that Nrf2 activation could counteract this pathophysiological mechanism by shifting the balance between Bmp6 and erythroferrone, stimulating the Bmp6-hepcidin axis. CDDO-Im was administered to th3/+ mice (a model of beta-thalassaemia intermedia[41]) and six hours later we noted increased hepatic *Bmp6* and other Nrf2 target genes *Nqo1, Gclc* and *Hmox1* and increased *Hamp1* in CDDO-Im treated th3/+ mice (Fig 6a). Splenic *Fam132b* mRNA (encoding erythroferrone), *Slc40a1* mRNA and kidney *Epo* mRNA were not altered by CDDO-Im (Fig 6b). Serum iron was markedly decreased in CDDO-Im treated th3/+ mice, while liver and spleen iron levels were not increased (Fig 6c). CDDO-Im–mediated Nrf2 activation augmented expression of *Bmp6* relative to its inhibitor erythroferrone, so increasing hepcidin and decreasing iron levels.

Overall, the Nrf2-Bmp6-erythroferrone axis responds to excess iron, oxidative damage, hypoxia and anaemia, and regulates iron homeostasis and iron toxicity (Fig 6d).

Discussion

Maintaining iron levels at sufficient but non-toxic concentrations is critical for health. In mammalian cells, elevated iron alters the conformation and stability of Iron Response Proteins (IRPs), regulating post-transcriptional expression of Iron Response Element (IRE)-containing genes and controlling cellular iron homeostasis[42]. However, the IRE-IRP system does not directly modify *Bmp6* expression[43], and the IRE-IRP cell-intrinsic iron homeostatic mechanisms and hepcidin-controlled systemic iron equilibrium are not directly linked[44]. We show instead that Nrf2 regulates *Bmp6* expression and is required for the induction of hepatic *Bmp6* in response to mitochondrial ROS and oxidative damage. Upon mitochondrial lipid peroxidation, electrophilic lipids are released from mitochondria and can react with cysteine residues on Keap1 to activate Nrf2[30]. Hence iron-induced mitochondrial oxidative damage likely activates Nrf2 (and increases *Bmp6* expression) by causing mitochondrial lipid peroxidation and the release of electrophilic reactive lipid species. In this model, 'toxic iron' rather than iron itself is the key entity influencing *Bmp6*-driven hepcidin synthesis. This mechanism may allow a distinction to be drawn between levels of iron accumulation that are not harmful and can be tolerated, and the development of potentially pathogenic iron overload. This sensing apparatus sits alongside hepatocytes that directly detect transferrin saturation via HFE and TFR2 to regulate hepcidin[1]. Thus both transferrin saturation sensing by hepatocytes and iron-driven LSEC Bmp6 synthesis (controlled by Nrf2) protect against iron accumulation.

However, *Nrf2*, unlike lack of *Hfe*, *Tfr2* or *Bmp6*, also regulates antioxidant defences. A single injection of iron dextran caused hepatic necroinflammation in *Nrf2*−/− mice but not wildtype controls, showing that iron is more cytotoxic in the absence of Nrf2. Iron-loaded *Nrf2*−/− mice demonstrated elevated liver lipid peroxidation and fibrotic markers; injured LSEC and hepatocyte mitochondria and disrupted sinusoid architecture were also apparent and likely caused by iron-induced mitochondrial oxidative damage. Oral and parenteral iron formulations, frequently administered worldwide for a range of conditions, cause varying degrees of transient labile non-transferrin bound iron that catalyses free-radical generation[10,45,46]. In our experiments, Nrf2 defends against oxidative damage and controls iron homeostasis in response to oral and parenteral iron.

Supraphysiological doses of recombinant BMP6 increase hepcidin and reduce serum iron in *Hfe*$^{-/-}$ mice[47], and increasing hepcidin in beta-thalassaemia is also therapeutic[48]. We activated Nrf2 with CDDO-Im in *Hfe*$^{-/-}$ mice and th3/+ mice and observed robust upregulation of *Bmp6* and hepcid in expression and decreased serum iron accumulation. Genes involved in the antioxidant response were also activated, and in *Hfe−/− mice* hepatic lipid peroxidation was decreased. Pharmacological Nrf2 activation in the context of iron overload boosts the capability to detoxify iron-induced ROS and stimulates the Bmp6-hepcidin axis. We demonstrate that Nrf2 links cellular health to systemic iron homeostasis, and constrains the cause and effects of iron-induced oxidative damage. This concept is relevant to a range of disease processes and treatments. Our findings suggest therapeutic

approaches for iron overload disorders, and extend the possible indications for Nrf2-activating drugs[49,50].

Methods

Mice

Unless otherwise stated, animal procedures were performed under the authority of UK Home office project and personal licenses in accordance with the Animals (Scientific Procedures) Act 1986, and were approved by the University of Oxford ethical review committee. Mice were housed in individually ventilated cages and fed *ad-libitum* with standard diet containing 188 ppm iron (SDS Dietex Services, diet 801161) C57BL/6 mice were purchased from Envigo. *Nrf2*$^{-/-}$ mice (RIKEN) were generated previously[51]. i*Hamp1*-KO mice were generated previously[19]. *Hfe*$^{-/-}$ mice were generated previously[52], backcrossed onto C57BL/6 background for 10 generations and were a kind gift from Helene Coppin (Toulouse, France). *Hamp1*$^{-/-}$ mice on a C57BL/6 background[53] were a kind gift from Sophie Vaulont (Institut Cochin, France); *Bmp6fl/fl;Tek-Cre*+ mice were generated previously[9].

Nrf2$^{+/+}$, *Nrf2*$^{+/-}$ and *Nrf2*$^{-/-}$ littermates treated with FeDx or carbonyl iron dietary loading, *Hfe*$^{-/-}$, *Bmp6fl/fl;Tek-Cre*+ and *Hamp1*$^{-/-}$ mice treated with CDDO-Im for 6 hours or 3 weeks, and *Hfe*/*Nrf2*$^{-/-}$ mice were bred and received humane care according to the EU Directive 2010/63/EU and the experimental procedures were approved by the *Instituto de Biologia Molecular e Celular* Animal Ethics Committee. LSECs isolation studies were approved by the Institutional Animal Care and Use Committee at Massachusetts General Hospital.

C57BL/6 mice heterozygous for the β-globin gene deletion (th3/+)[41] were maintained and bred in the animal facility at the Lady Davis Institute for Medical Research. The th3/+ mice were used as a model of thalassemia intermedia[41] and were kindly donated by Stefano Rivella.

Mouse treatments

Dietary iron loading: Mice were fed 200ppm iron control diet (Harlan, TD.07801), 1% carbonyl iron diet (Harlan, TD.09077) or 2% carbonyl iron diet (Harlan, 2018S) *ad-libitum*; diets were matched for other constituents. For LSEC isolation studies, wildtype 129S6/SvEvTac male mice were fed control 37ppm iron or 1% carbonyl iron diets (Research Diets) for 4 weeks. Iron-dextran (FeDx): Mice were given intraperitoneal (i.p.) injections of FeDx (Sigma, D8517) or dextran Dx control (Sigma, D9260) for 6 or 24 hours. i*Hamp1*-knockout: i*Hamp1*-Ctrl and i*Hamp1*KO mice were given 1mg tamoxifen (Sigma, T5648) in 90% Corn Oil / 10% Ethanol i.p. for 4 consecutive days. Ferrous sulphate: Mice were fed 2ppm iron diet *ad-libitum* for 3 weeks, followed by oral gavage with 2mg/kg elemental iron (as $FeSO_4$) (Sigma, F7002) and culled 6 hours later. Hemin: Mice were administered two i.p. doses of 50μmol/kg hemin (Sigma, 512800) or saline 12-hours apart and culled 12 hours after the last dose. mitoTEMPO: 0.25mg mitoTEMPO (Sigma, SML0737) in saline was administered i.p. 1 hour after gavage with 2mg/kg elemental iron (as $FeSO_4$) and culled 6 hours later. CDDO-

Imidazole (CDDO-Im): Mice were given 30μmol/kg CDDO-Im (Tocris Bioscience, 4737) dissolved in DMSO and reconstituted in PBS / 5% Tween80 / 5% PEG300 by oral gavage. Mice were culled in increasing CO_2. Tissues were harvested for non-heme iron measurement, gene expression, Nrf2 protein, and histology analysis. Serum was collected for iron and hepcidin measurements.

Cell cultures

L929 fibroblast, C2C12 myoblast and MEF mouse embryonic fibroblast cells were maintained in Dulbecco's modified Eagle's medium (*DMEM)* supplemented with 10% fetal calf serum (FCS), 2mM glutamine, 100U/ml penicillin and 0.1mg/ml streptomycin. CD1 mouse primary liver sinusoidal endothelial cells (Cell Biologics) were maintained in complete mouse endothelial cell medium with growth factor supplement following manufacturer's instructions. The LSEC cell line (TMNK-1[54]) was kindly provided by Dr Naoya Kobayashi at the Department of Surgery, Okayama University Graduate School of Medicine and Dentistry, Okayama, Japan.

In vitro treatments

siRNA-mediated knockdown was performed with Lipofectamine RNAiMAX reagent with 100nM Dharmacon siGENOME SMARTpool siRNA targeting mouse Nrf2 (M-040766-01-0005), Keap1 (M-041104-01-0005) or Bach1 (M-042956-01-0005) in antibiotic-free media for 24 hours (Nrf2) or 48 hours (Keap1 and Bach1). L929 cells were treated with 0.1mg/ml or 1mg/ml FeDx with or without 500μM mitoTEMPO, 2μM or 10μM hemin. C2C12, MEF and mouse primary LSECs were treated with 200μg/ml ferric ammonium citrate, FAC (Sigma). LSECs were treated with 100nM CDDO-Im (Tocris Bioscience). Cells were harvested for Western blot and/or qRT-PCR analysis. MitoPQ was synthesised as described[29] and used at 100uM; the mitochondria targeted MitoPQ control compound was also used at 100uM and has been described[31], and its full synthesis will be published separately. LSEC cell line (TMNK-1) was cultured in Dulbecco's modified Eagle's medium (DMEM) (Gibco) supplemented with 10% fetal bovine serum (FBS), 100U/ml penicillin, 0.1mg/ml streptomycin, 2mM L-glutamine (Sigma Aldrich) and non essentional amino acids NEAA (Invitrogen); cells were passaged twice a week using trypsin EDTA (Sigma). LSECs were plated at 0.1×10e6/well in 100 uL of culture Medium in 96 well flat bottom plate +/− CDDO-Im or +/− FAC as indicated.

LSEC isolation

Livers were dissected after cardiac perfusion with 25 ml sterile PBS. Single cell suspension was made by incubating scissor cut 200mg liver 10minutes at 37°C in 1ml cocktail containing 450U/ml collagenase I, 125U/ml collagenase XI, 60U/ml Dnase I, 60U/ml Hyaluronidase and 20mM HEPES (Sigma-Aldrich). After cell suspension was filtered through 40 μm cell strainer, non-parenchymal cells were pelleted down at 750 x g for 7minutes at 4°C and resuspended with PBS containing 1% FBS and 0.5% BSA. The following monoclonal antibodies were used for cell sorting: anti-Ly-6C (clone AL-21, BD Biosciences), anti-CD45.2 (clone 104, BD Biosciences), anti-CD3e (clone 145– 2C11, ebioscience), anti-CD90.2 (clone 53–2.1, BD Biosciences), anti-CD19 (clone 6D5, Biolegend), anti-MHC-II (clone AF6–120.1, BD Biosciences), anti-F4/80 (clone BM8,

Biolegend), anti-NK1.1 (clone PK136, BD Biosciences), anti-Ly-6G (clone 1A8, BD Biosciences), anti-CD11b (clone M1/70, BD Biosciences), anti-CD146 (clone ME-9F1, BioLegend), anti-CD31 (clone 390, BioLegend), anti-CD326 (clone G8.8, BioLegend), anti-CD64 (clone X54–5/7.1, BioLegend). Cells were first gated using FSC/SSC characteristics, and doublets were sequentially excluded by comparing FSC- and SSC-height and -area signals. Specifically, endothelial cells were identified as CD45-, CD31+, Lin-, MHCII-, CD64-, CD146+. Lineage was defined as: CD3e, CD19, CD90.2, CD326, Ly6G, NK1.1. Cells were sorted on a FACSAria II (BD Biosciences). See Supplementary Figure 9 for FACS gating strategy, and Supplementary Table 1 for details of antibodies used.

Western blot

Cells were pelleted for nuclear and cytoplasmic fractionation using the NEPER protein extraction kit (Thermo Scientific, 78833). Whole cell extracts were harvested using the RIPA lysis buffer (ThermoFisher, 89900) with protease and phosphatase inhibitor cocktail. Liver tissues were agitated with glass beads (Sigma, G8772) and lysed in RIPA buffer (ThermoFisher, 89900). Proteins were separated by 10% SDS-polyacrylamide gel electrophoresis, transferred onto 0.2μm nitrocellulose membrane, and probed with antibodies against Nrf2 (Cell Signaling Technology, D1Z9C), Bach1 (R&D systems, AF5777), lamin A (Abcam, ab8980), and GAPDH (Proteintech, 60004). See Supplementary Figure 10 for all uncropped gels, and Supplementary Table 1 for details of antibodies used.

Gene expression analysis by quantitative real time PCR (qRT-PCR)

RNA was extracted from liver explants and cells with RNeasy plus kit (Qiagen, 74136) and reverse transcribed to cDNA (Life Technologies, 4387406) for quantitative PCR on the Applied Biosystems 6500 Fast Real-Time PCR system machine using TaqMan assays listed in Supplementary Table 2 according to the manufacturers' protocols, except for *Hfe*/*Nrf2*$^{-/-}$ and LSEC isolation experiments. In *Hfe*/*Nrf2*$^{-/-}$ experiment, RNA was extracted using TriZol, DNase-treated, and reverse transcribed to cDNA (ThermoScript RT-PCR System). Relative gene expression levels were quantified using iQ5 Real-Time PCR Detection System. All reactions were performed with iQ SYBR Green Supermix, with primers listed in Suplementary Table 3. The quantity of each transcript was estimated against the respective standard curve and normalized against the quantity of the endogenous control gene Hypoxanthine phosphoribosyltransferase 1 (*Hprt1*). In LSECs experiments, total RNA was isolated using PicoPure RNA Isolation Kit (Thermo Scientific). cDNA was synthesized using the SuperScript VILO cDNA Synthesis Kit (Invitrogen). PCR reactions were carried out by using the PowerUp SYBR Green Master Mix (Applied Biosystems) on the QuantStudio3 Real-Time PCR system (Applied Biosystems), with primers listed in Supplementary Table 4.

Tissue non-heme iron measurement

Tissue samples were dried for 4–6 h at 100 °C before weighing. Dried tissue was digested with 10% trichloroacetic acid/30% hydrochloric acid for 20 h at 65 °C. Non-heme iron content was measured colorimetrically (OD 535 nm) against a standard curve generated from ferric ammonium citrate (F5879, Sigma) serial dilutions following reaction with

chromogen reagent containing 0.1% (w/v) batho-phenoldisulphonic acid (BPS, 146617, Sigma)/0.8% thioglycolic acid (88652, Sigma).

Tissue histology

Liver and spleen samples from *Hfe*$^{-/-}$ mice given CDDO-Im, liver tissue from *Nrf2*$^{-/-}$ mice injected with FeDx, and liver, heart and pancreas tissues from *Hfe*/*Nrf2*$^{-/-}$ mice were fixed in neutral formalin 10% and embedded in paraffin. 3μm-thick sections were stained with Perls' Prussian blue reaction for ferric iron using standard procedures at Ipatimup Diagnostics (Ipatimup, Porto, Portugal).

Transmission electron microscopy

Liver tissue samples were immersed immediately on isolation into 2.5% glutaraldehyde in 0.1 M cacodylate buffer (pH 7.4) overnight and then postfixed in 2.0% osmium tetroxide for 2 h, dehydrated through a series of ethanol solutions, and embedded in Epon. Ultrathin sections (50 nm) stained with uranyl acetate and lead citrate were visualized with a JEM 1400 electron microscope (Jeol, Tokyo, Japan) operated at 120 kV. Electron micrographs were captured with an Orius CCD (Gatan, Warrendale, PA, USA).

Liver malondialdehyde (MDA)

Liver tissues were agitated with glass beads (Sigma, G8772) and lysed in RIPA buffer (ThermoFisher, 89900). Lysates were used for quantification of MDA using the thiobarbaturic acid reactive substance (TBARS) kit according to the manufacturer's protocols (Cayman Chemical, 700870). Briefly, liver lysates were allowed to react with thiobarbaturic acid at 95°C for 1 hour, and absorbance of the solution was measured at 530nm.

Serum measurements

Blood was taken by cardiac puncture immediately after euthanising mice. Serum was prepared by centrifugation of clotted blood at 8000 x g for 5minutes in BD Microtainer SST tubes (Beckton Dickinson). Serum hepcidin was quantified by competitive ELISA using the Hepcidin-Murine Compete Kit (Intrinsic Lifesciences) according to the manufacturer's protocol. For mice given $FeSO_4$ gavage, serum iron was quantified using the MULTIGENT Iron Kit on the Abbott Architect c16000 automated analyzer (Abbott Laboratories) at John Radcliffe Hospital, UK. For *Hfe*$^{-/-}$ and *Hamp1*$^{-/-}$ mice given CDDO-Im, serum irons were quantified in a Cobas C8000 analyzer (Roche Diagnostics, Mannheim, Germany) at *Centro Hospitalar do Porto*.

ChIP-sequencing

Previously published Nrf2 ChIP-seq datasets generated from differentiated C2C12 myotube cells treated with 100nM CDDO-Im for 3 hours[22] and from *Keap1*-knockout MEF cells[55] were mapped onto the mouse mm9 genome build on UCSC genome browser. ChIP-seq tracks of H3K4-monomethylation (H3K4me1) depicting enhancer regions, H3K4-trimethylation (H3K4me3) depicting promoter regions, and RNA polymerase II (RNA pol

II) on MEF cells, as well as mammalian conservation based on multiple alignments of 30 vertebrate species were also mapped onto the mm9 mouse genome.

Statistics

Standard randomization procedures were used for cell-line groups and mice of the same age and sex (experimental and control mice were chosen at random from among littermates). The investigators were not blinded to allocation during experiments and assessments. The required number of mice for each experiment was determined from availability of bred animals, power calculations, prior experience of performing experiments with the same strains of mice and data from pilot experiments. Statistical analyses were performed using Prism version 6 (GraphPad Software). Details of specific statistical tests are given in figure legends.

Supplementary Material

Refer to Web version on PubMed Central for supplementary material.

Acknowledgements

The authors thank the staff of the University of Oxford Department of Biomedical Services for animal husbandry, Manfred Nairz (Medical University of Innsbruck, Austria) for assistance with flow cytometry, and Alain Townsend (WIMM, Oxford, UK) for helpful advice and discussions. This work was supported by the Medical Research Council UK (MRC Human Immunology Unit core funding to HD) and Radcliffe Department of Medicine (RDM Scholars Program to PJL). The work conducted at the Instituto de Biologia Molecular e Celular was supported by FEDER funds through COMPETE - and by Portuguese funds through Fundação para a Ciência e Tecnologia (PTDC/BIM-MET/0739/2012 and SFRH/BPD/108207/2015 to TLD), and by Norte 2020 Portugal Regional Operational Programme (Norte-01-0145-FEDER-000012). RCH's lab is support by a Wellcome Trust Investigator award (110158/Z/15/Z). JLB is supported by National Institutes of Health (RO1-DK087727 to JLB), Massachusetts General Hospital (Howard Goodman Award to JLB). Work in MPM's lab is supported by the Medical Research Council UK (MC_U105663142) and by a Wellcome Trust Investigator award (110159/Z/15/Z). AMH, DGS and PP were funded by grants from the Canadian Institutes of Health Research (MOP-14100 and MOP-126064).

References:

1. Muckenthaler MU, Rivella S, Hentze MW & Galy B A Red Carpet for Iron Metabolism. Cell 168, 344–361, 10.1016/j.cell.2016.12.034 (2017). [PubMed: 28129536]
2. Ganz T Systemic iron homeostasis. Physiological reviews 93, 1721–1741, 10.1152/physrev.00008.2013 (2013). [PubMed: 24137020]
3. Nemeth E et al. Hepcidin regulates cellular iron efflux by binding to ferroportin and inducing its internalization. Science 306, 2090–2093 (2004). [PubMed: 15514116]
4. Pietrangelo A Genetics, Genetic Testing, and Management of Hemochromatosis: 15 Years since Hepcidin. Gastroenterology 149, 1240–1251e1244, 10.1053/j.gastro.2015.06.045 (2015). [PubMed: 26164493]
5. Gupta R, Musallam KM, Taher AT & Rivella S Ineffective Erythropoiesis: Anemia and Iron Overload. Hematology/oncology clinics of North America 32, 213–221, 10.1016/j.hoc.2017.11.009 (2018). [PubMed: 29458727]
6. Kautz L et al. Iron regulates phosphorylation of Smad1/5/8 and gene expression of Bmp6, Smad7, Id1, and Atoh8 in the mouse liver. Blood 112, 1503–1509 (2008). [PubMed: 18539898]
7. Andriopoulos B Jr. et al. BMP6 is a key endogenous regulator of hepcidin expression and iron metabolism. Nat Genet 41, 482–487 (2009). [PubMed: 19252486]
8. Meynard D et al. Lack of the bone morphogenetic protein BMP6 induces massive iron overload. Nat Genet 41, 478–481 (2009). [PubMed: 19252488]

9. Canali S et al. Endothelial cells produce bone morphogenetic protein 6 required for iron homeostasis in mice. Blood 129, 405–414, 10.1182/blood-2016-06-721571 (2017). [PubMed: 27864295]
10. Koskenkorva-Frank TS, Weiss G, Koppenol WH & Burckhardt S The complex interplay of iron metabolism, reactive oxygen species, and reactive nitrogen species: Insights into the potential of various iron therapies to induce oxidative and nitrosative stress. Free Radic Biol Med 65C, 1174–1194, 10.1016/j.freeradbiomed.2013.09.001 (2013).
11. Hershko C Pathogenesis and management of iron toxicity in thalassemia. Annals of the New York Academy of Sciences 1202, 1–9, 10.1111/j.1749-6632.2010.05544.x (2010). [PubMed: 20712765]
12. Suzuki T & Yamamoto M in Free Radical Biology and Medicine Vol. 88 93–100 (2015). [PubMed: 26117331]
13. Kobayashi A et al. Oxidative and electrophilic stresses activate Nrf2 through inhibition of ubiquitination activity of Keap1. Molecular and cellular biology 26, 221–229, 10.1128/MCB.26.1.221-229.2006 (2006). [PubMed: 16354693]
14. Igarashi K & Watanabe-Matsui M Wearing red for signaling: the heme-bach axis in heme metabolism, oxidative stress response and iron immunology. Tohoku J. Exp. Med, 229–253, 10.1620/tjem.232.229.Correspondence (2013). [PubMed: 24240713]
15. Kautz L et al. BMP/Smad signaling is not enhanced in Hfe-deficient mice despite increased Bmp6 expression. Blood 114, 2515–2520 (2009). [PubMed: 19622835]
16. Ryan JD, Ryan E, Fabre A, Lawless MW & Crowe J Defective bone morphogenic protein signaling underlies hepcidin deficiency in HFE hereditary hemochromatosis. Hepatology 52, 1266–1273, 10.1002/hep.23814 (2010). [PubMed: 20658468]
17. Moon MS et al. Elevated hepatic iron activates NF-E2-related factor 2-regulated pathway in a dietary iron overload mouse model. Toxicological sciences : an official journal of the Society of Toxicology 129, 74–85, 10.1093/toxsci/kfs193 (2012). [PubMed: 22649188]
18. Silva-Gomes S et al. Transcription factor NRF2 protects mice against dietary iron-induced liver injury by preventing hepatocytic cell death. Journal of Hepatology 60, 354–361, 10.1016/j.jhep.2013.09.004 (2014). [PubMed: 24021424]
19. Armitage AE et al. Induced disruption of the iron-regulatory hormone hepcidin inhibits acute inflammatory hypoferremia Journal of Innate Immunity (2016).
20. Liby K et al. The synthetic triterpenoids, CDDO and CDDO-imidazolide, are potent inducers of heme oxygenase-1 and Nrf2/ARE signaling. Cancer research 65, 4789–4798, 10.1158/0008-5472.CAN-04-4539 (2005). [PubMed: 15930299]
21. Cleasby A et al. Structure of the BTB domain of Keap1 and its interaction with the triterpenoid antagonist CDDO. PloS one 9, e98896, 10.1371/journal.pone.0098896 (2014). [PubMed: 24896564]
22. Uruno A et al. Nrf2-Mediated Regulation of Skeletal Muscle Glycogen Metabolism. Molecular and Cellular Biology 36, 1655–1672, 10.1128/MCB.01095-15 (2016). [PubMed: 27044864]
23. Yamamoto T et al. Predictive base substitution rules that determine the binding and transcriptional specificity of Maf recognition elements. Genes to Cells 11, 575–591, 10.1111/j.1365-2443.2006.00965.x (2006). [PubMed: 16716189]
24. Reichard JF, Motz GT & Puga A Heme oxygenase-1 induction by NRF2 requires inactivation of the transcriptional repressor BACH1. Nucleic Acids Research 35, 7074–7086, 10.1093/nar/gkm638 (2007). [PubMed: 17942419]
25. Mills EL et al. Itaconate is an anti-inflammatory metabolite that activates Nrf2 via alkylation of KEAP1. Nature 556, 113–117, 10.1038/nature25986 (2018). [PubMed: 29590092]
26. Urrutia PJ, Mena NP & Nunez MT The interplay between iron accumulation, mitochondrial dysfunction, and inflammation during the execution step of neurodegenerative disorders. Frontiers in pharmacology 5, 38, 10.3389/fphar.2014.00038 (2014). [PubMed: 24653700]
27. Huang H et al. Iron-induced generation of mitochondrial ROS depends on AMPK activity. Biometals : an international journal on the role of metal ions in biology, biochemistry, and medicine 30, 623–628, 10.1007/s10534-017-0023-0 (2017).
28. Liang HL et al. Partial attenuation of cytotoxicity and apoptosis by SOD1 in ischemic renal epithelial cells. Apoptosis : an international journal on programmed cell death 14, 1176–1189, 10.1007/s10495-009-0393-z (2009). [PubMed: 19685188]

29. Robb EL et al. Selective superoxide generation within mitochondria by the targeted redox cycler MitoParaquat. Free Radic Biol Med 89, 883–894, 10.1016/j.freeradbiomed.2015.08.021 (2015). [PubMed: 26454075]
30. Higdon A, Diers AR, Oh JY, Landar A & Darley-Usmar VM Cell signalling by reactive lipid species: new concepts and molecular mechanisms. The Biochemical journal 442, 453–464, 10.1042/BJ20111752 (2012). [PubMed: 22364280]
31. Fazakerley DJ et al. Mitochondrial oxidative stress causes insulin resistance without disrupting oxidative phosphorylation. The Journal of biological chemistry, 10.1074/jbc.RA117.001254 (2018).
32. Yanagawa T et al. Nrf2 deficiency causes tooth decolourization due to iron transport disorder in enamel organ. Genes to cells : devoted to molecular & cellular mechanisms 9, 641–651, 10.1111/j.1356-9597.2004.00753.x (2004). [PubMed: 15265007]
33. Marro S et al. Heme controls ferroportin1 (FPN1) transcription involving Bach1, Nrf2 and a MARE/ARE sequence motif at position −7007 of the FPN1 promoter. Haematologica 95, 1261–1268, 10.3324/haematol.2009.020123 (2010). [PubMed: 20179090]
34. Jenkitkasemwong S et al. SLC39A14 Is Required for the Development of Hepatocellular Iron Overload in Murine Models of Hereditary Hemochromatosis. Cell metabolism 22, 138–150, 10.1016/j.cmet.2015.05.002 (2015). [PubMed: 26028554]
35. Lebeau A et al. Long-term sequelae of HFE deletion in C57BL/6 × 129/O1a mice, an animal model for hereditary haemochromatosis. European journal of clinical investigation 32, 603–612 (2002). [PubMed: 12190960]
36. Duarte TL et al. Genetic disruption of NRF2 promotes the development of necroinflammation and liver fibrosis in a mouse model of HFE-hereditary hemochromatosis. Redox biology 11, 157–169, 10.1016/j.redox.2016.11.013 (2017). [PubMed: 27936457]
37. Koch PS et al. Angiocrine Bmp2 signaling in murine liver controls normal iron homeostasis. Blood 129, 415–419, 10.1182/blood-2016-07-729822 (2017). [PubMed: 27903529]
38. Kohler UA et al. Activated Nrf2 impairs liver regeneration in mice by activation of genes involved in cell-cycle control and apoptosis. Hepatology 60, 670–678, 10.1002/hep.26964 (2014). [PubMed: 24310875]
39. Kautz L et al. Identification of erythroferrone as an erythroid regulator of iron metabolism. Nat Genet 46, 678–684, 10.1038/ng.2996 (2014). [PubMed: 24880340]
40. Arezes J et al. Erythroferrone inhibits the induction of hepcidin by BMP6. Blood 132, 1473–1477, 10.1182/blood-2018-06-857995 (2018). [PubMed: 30097509]
41. Yang B et al. A mouse model for beta 0-thalassemia. Proceedings of the National Academy of Sciences of the United States of America 92, 11608–11612 (1995). [PubMed: 8524813]
42. Wilkinson N & Pantopoulos K The IRP/IRE system in vivo: insights from mouse models. Frontiers in pharmacology 5, 176, 10.3389/fphar.2014.00176 (2014). [PubMed: 25120486]
43. Sanchez M et al. Iron regulatory protein-1 and −2: transcriptome-wide definition of binding mRNAs and shaping of the cellular proteome by iron regulatory proteins. Blood 118, e168–179, 10.1182/blood-2011-04-343541 (2011). [PubMed: 21940823]
44. Hentze MW, Muckenthaler MU, Galy B & Camaschella C Two to tango: regulation of Mammalian iron metabolism. Cell 142, 24–38 (2010). [PubMed: 20603012]
45. Bhandari S, Pereira DIA, Chappell HF & Drakesmith H Intravenous Irons: From Basic Science to Clinical Practice. Pharmaceuticals 11, 10.3390/ph11030082 (2018).
46. Brittenham GM et al. Circulating non-transferrin-bound iron after oral administration of supplemental and fortification doses of iron to healthy women: a randomized study. The American journal of clinical nutrition 100, 813–820, 10.3945/ajcn.113.081505 (2014). [PubMed: 25057155]
47. Corradini E et al. BMP6 treatment compensates for the molecular defect and ameliorates hemochromatosis in Hfe knockout mice. Gastroenterology 139, 1721–1729, 10.1053/j.gastro.2010.07.044 (2010). [PubMed: 20682319]
48. Casu C et al. Minihepcidin peptides as disease modifiers in mice affected by beta-thalassemia and polycythemia vera. Blood 128, 265–276, 10.1182/blood-2015-10-676742 (2016). [PubMed: 27154187]

49. Bollong MJ et al. A metabolite-derived protein modification integrates glycolysis with KEAP1-NRF2 signalling. Nature 562, 600–604, 10.1038/s41586-018-0622-0 (2018). [PubMed: 30323285]
50. Dodson M et al. Modulating NRF2 in Disease: Timing Is Everything. Annual review of pharmacology and toxicology, 10.1146/annurev-pharmtox-010818-021856 (2018).
51. Itoh K et al. An Nrf2/small Maf heterodimer mediates the induction of phase II detoxifying enzyme genes through antioxidant response elements. Biochemical and biophysical research communications 236, 313–322, 10.1006/bbrc.1997.6943 (1997). [PubMed: 9240432]
52. Bahram S et al. Experimental hemochromatosis due to MHC class I HFE deficiency: immune status and iron metabolism. Proceedings of the National Academy of Sciences of the United States of America 96, 13312–13317 (1999). [PubMed: 10557317]
53. Lesbordes-Brion JC et al. Targeted disruption of the hepcidin 1 gene results in severe hemochromatosis. Blood 108, 1402–1405, 10.1182/blood-2006-02-003376 (2006). [PubMed: 16574947]
54. Matsumura T et al. Establishment of an immortalized human-liver endothelial cell line with SV40T and hTERT. Transplantation 77, 1357–1365 (2004). [PubMed: 15167590]
55. Malhotra D et al. Global mapping of binding sites for Nrf2 identifies novel targets in cell survival response through ChIP-Seq profiling and network analysis. Nucleic Acids Research 38, 5718–5734, 10.1093/nar/gkq212 (2010). [PubMed: 20460467]

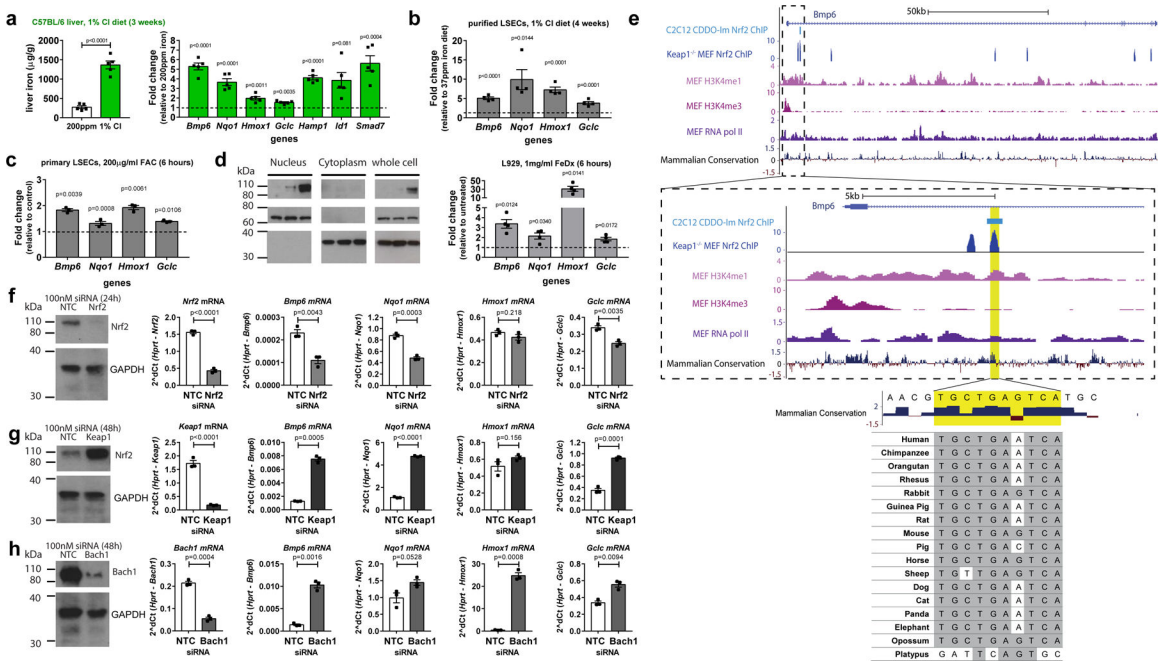

Figure 1.

The transcription factor Nrf2 regulates *Bmp6* gene expression. **(a)** 3-week old C57BL/6 male mice were fed 3 weeks of control (200ppm iron) or high iron diet (1% CI). Liver non-heme iron content and hepatic gene expression of *Bmp6*, well-characterised Nrf2 target genes (*Nqo1*, *Hmox1* and *Gclc*) and Bmp-Smad target genes (*Hamp1*, *Id1* and *Smad7*) were quantified (n=5 mice). **(b)** Liver sinusoidal endothelial cells (LSECs) were purified from mice fed 4 weeks control (37ppm iron) or high iron diet containing 1% carbonyl iron (CI). Gene expression was quantified by qRT-PCR (n=4 mice). (**c**) Primary LSECs were cultured with 200ug/mL ferric ammonium citrate (FAC) for 6 hours and expression of *Bmp6, Nqo1, Hmox1* and *Gclc* was quantified (n=3 biologically independent samples). **(d)** L929 cells were treated with iron-dextran (FeDx) for 6 hours. Nrf2 protein was detected by Western blot in nuclear, cytoplasmic and whole cell extracts, with lamin A as nuclear marker and GAPDH as cytoplasmic marker. Gene expression of *Bmp6*, *Nqo1*, *Hmox1* and *Gclc* was quantified by qRT-PCR (n=4 biologically independent samples). **(e)** Nrf2 ChIP-seq datasets from C2C12 cells treated with CDDO-Im for 3 hours and *Keap1*-knockout MEF cells, ChIP-seq tracks of H3K4- monomethylation (H3K4me1) depicting enhancer regions, H3K4-trimethylation (H3K4me3) depicting promoter regions, and RNA polymerase II (RNA pol II) on MEF cells, as well as mammalian conservation based on multiple alignments of 30 vertebrate species were mapped onto the mm9 mouse genome build on UCSC genome browser. The consensus ARE sequence in intron1 of *Bmp6* is highlighted in yellow. **(f-h)** siRNA-mediated knockdown of **(f)** Nrf2, **(g)** Keap1 and **(h)** Bach1 was performed in MEF cells. Knockdown efficiency was validated by Western blot and qRT- PCR. Gene expression of *Bmp6*, *Nqo1*, *Hmox1* and *Gclc* was quantified by qRT-PCR (n=3 biologically independent samples). Data represented with centre values as mean and error bars as SEM. Two-tailed t-tests performed between iron-treated and control groups, and between NTC and Nrf2/Keap1/Bach1 siRNA groups.

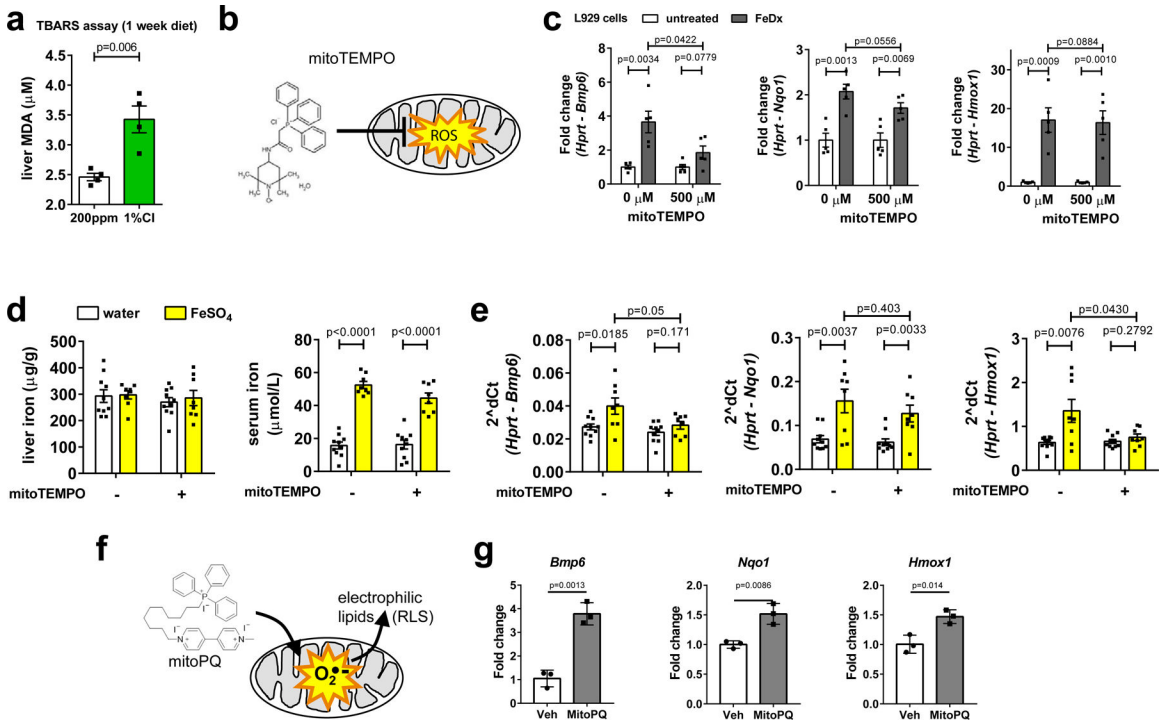

Figure 2.

Iron induces oxidative stress to activate Nrf2 and upregulate *Bmp6* expression. **(a)** 7-week old C57BL/6 male mice were fed control (200ppm iron) or high iron diet (1% CI) for a week. Hepatic malondialdehyde (MDA) was quantified by the Thiobarbituric acid reactive substances (TBARS) assay (n=4 mice). **(b)** MitoTEMPO decreases mitochondrial oxidative damage. (**c**) L929 cells were pretreated with 500μM mitoTEMPO for 1 hour, followed by 1mg/ml FeDx for 6 hours. Gene expression of *Bmp6*, *Nqo1* and *Hmox1* was quantified by qRT-PCR (n=5 biologically independent samples). **(d,e)** 4-week old C57BL/6 male mice were fed 2ppm iron diet for 3 weeks, gavaged with 2mg/kg iron ($FeSO_4$), injected with 0.25mg mitoTEMPO 1 hour after iron gavage, and sacrificed 5 hours after mitoTEMPO injection (n=10 (water-treated groups), n=8 ($FeSO_4$-treated groups) mice). (**d**) Liver non-heme iron and serum iron and (**e**) hepatic gene expression was quantified. (**f**) Mito- Paraquat (mitoPQ) localises to mitochondria, selectively induces superoxide and leads to selective mitochondrial oxidative damage release of electrophilic reactive lipid species (RLS). (**g**) C2C12 cells were exposed to 100uM mitoPQ for 6 hours and then gene expression was quantified (n=3 biologically independent samples). Data represented with centre values as mean and error bars as SEM. Statistics: Two-tailed t-tests.

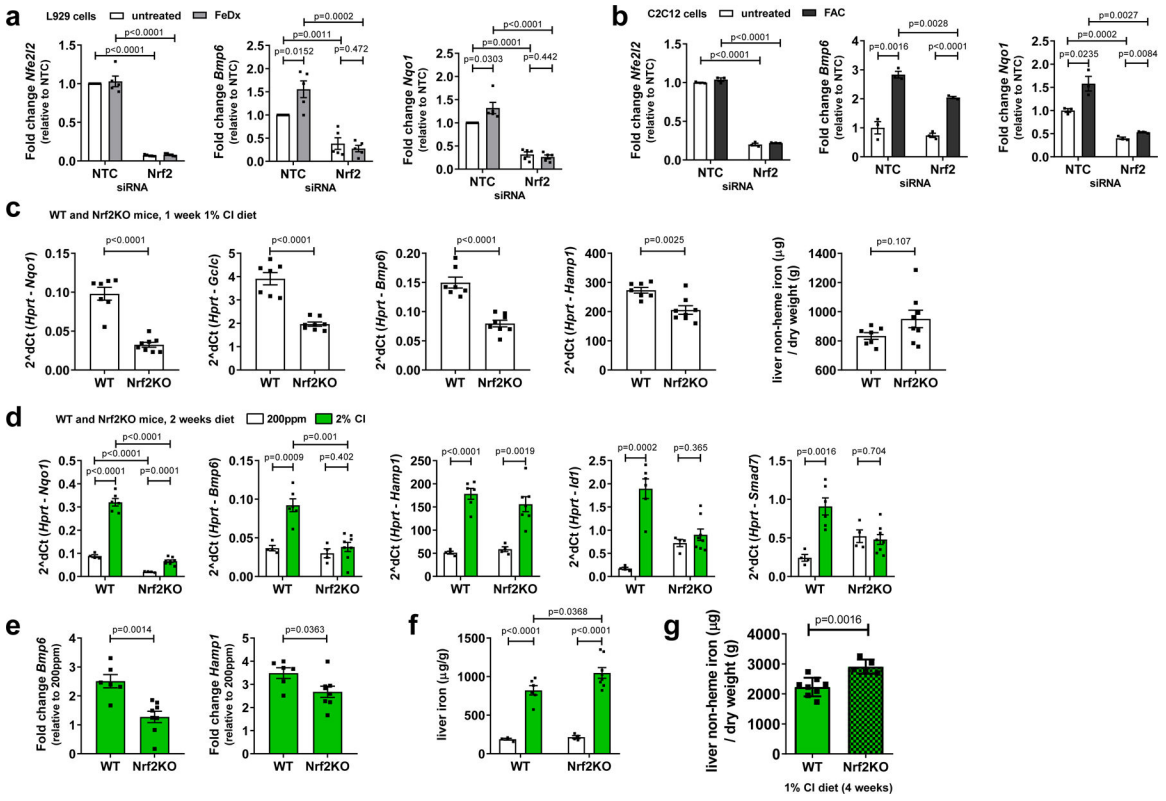

Figure 3.

Induction of *Bmp6* and hepcidin by iron is blunted in the absence of Nrf2; *Nrf2*-knockout mice load with more hepatic iron. **(a)** Nrf2 was knocked-down for 24 hours, followed by 1mg/ml FeDx treatment for 6 hours in L929 cells. Gene expression of *Nfe2l2*, *Bmp6* and *Nqo1* was quantified by qRT-PCR (n=5 biologically independent experiments). **(b)** Nrf2 was knocked-down for 24 hours, followed by 200µg/ml FAC treatment for 6 hours in C2C12 cells. Gene expression of *Nfe2l2*, *Bmp6* and *Nqo1* was quantified by qRT-PCR (n=5 biologically independent experiments). (**c**) wild-type and *Nrf2*−/− mice were fed 1% carbonyl iron diet for one week, and then hepatic gene expression of *Nqo1, Gclc, Bmp6* and *Hamp1* was quantified, and liver non-heme iron levels were measured (n=7 (WT) and n=8 (*Nrf2*−/−) mice). **(d-f)** 12-week old male *Nrf2*-knockout and wildtype littermate mice were fed 200ppm iron or 2% CI diet for 2 weeks. **(d)** Hepatic gene expression of *Nqo1*, *Bmp6*, *Hamp1*, *Id1* and *Smad7* was quantified by qRT-PCR (n=4 (WT 200ppm, *Nrf2*−/− 200ppm), n=6 (WT 2%CI) and n=8 (*Nrf2*−/− 2%CI) mice). **(e)** Fold change in hepatic *Bmp6* and *Hamp1* was calculated in mice fed 2% CI diet relative to mice fed 200ppm iron diet within each genotype. **(f)** Liver non-heme iron content was quantified. **(g)** 4-week old male *Nrf2*−/− and wildtype littermate mice were fed 1% CI diet for 4 weeks (n=8 (WT) and n=5 (*Nrf2*−/−) mice) and non-heme liver iron was quantified. Data represented with centre values as mean and error bars as SEM. Statistics: **(a)** two-tailed paired t-test and **(b-g)** two- tailed t-test

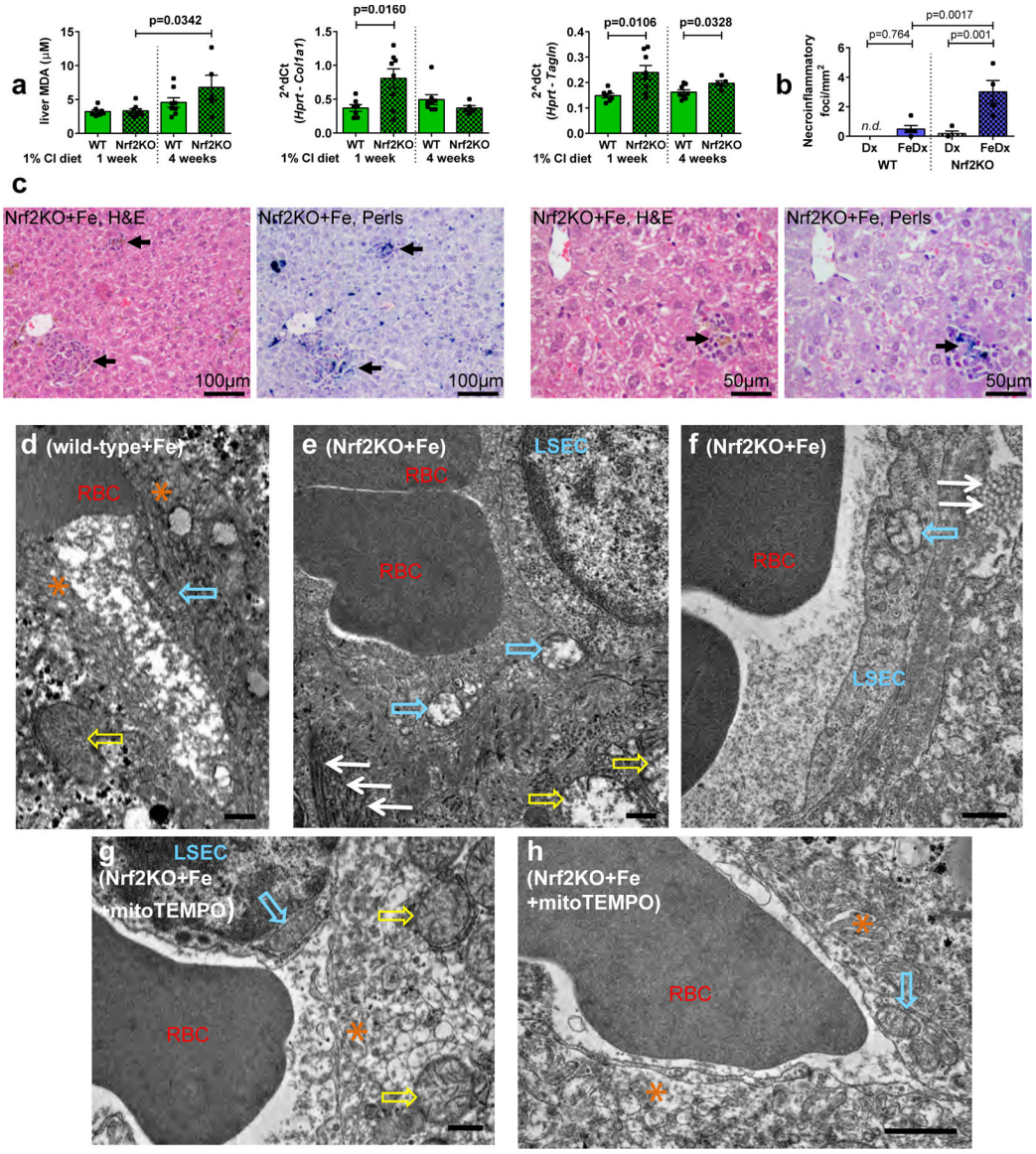

Figure 4.

Liver and LSEC mitochondrial pathology in iron loaded *Nrf2*−/− mice. (**a**) 7-week and 4-week old male *Nrf2*-knockout and wildtype littermate mice were fed 1% CI diet for 1 week (n=7 (WT), n=8 (*Nrf2*−/−) mice) or 4 weeks (n=8 (WT), n=5 (*Nrf2*−/−) mice), respectively, and culled at 8- week old. Malondialdehyde (MDA) and gene expression of *Col1a1* and *Tagln* was quantified. **(b)** *Nrf2*−/− and WT mice were given a single intraperitoneal injection of 4mg FeDx or Dx. Liver necroinflammatory foci were quantified 30 days post-injection (n=5 (WT) and n=4 (*Nrf2*−/−) mice); (**c**) representative liver sections stained with HE (first, third images) or Perls Prussian blue (second, fourth images), necroinflammatory foci in *Nrf2*−/− mouse livers at 30 days post-FeDx injection containing hepatocyte apoptotic bodies and iron pigment in histiocytes are shown (arrows). (**d**) Transmission electron microscopy (TEM) of a liver sinusoid of a WT mouse fed iron-rich diet (2% CI) for 2 weeks (representative of n=3 mice) depicting intact mitochondria in an LSEC (blue arrow) and

adjacent hepatocyte (yellow arrow), and hepatocyte microvilli (orange *). (**e,f**) TEM of hepatic sinusoidal areas of *Nrf2*−/− mice on the same diet (representative of n=3 mice), showing deposition of extracellular matrix proteins in Disse's spaces (white arrows), with continuous basement membranes evident on the basal side of LSECs. Note the presence of mitochondrial injuries in both LSECs (blue arrows) and hepatocytes (yellow arrows), including mitochondrial swelling and loss of cristae. (**g,h**) In *Nrf2*−/− mice fed iron-rich diet and treated daily with mitoTEMPO (10 mg/kg intraperitoneally for 2 weeks, from the day before the start of dietary iron supplementation) (representative of n=3 mice), microvilli of the hepatocytes extend into the space of Disse (*) and sinusoids are lined by fenestrated, incomplete endothelium. The mitochondria of LSECs and hepatocytes (blue and yellow arrows, respectively) are better preserved with evident matrix and cristae. Images from d-h are representative of 3 mice. Stain, uranyl acetate and lead citrate; scale bar, 0.5 μm. LSEC, liver sinusoidal endothelial cell; RBC, red blood cell. Data in **a, b** represented with centre values as mean and error bars as SEM. Statistics: two-tailed t-test.

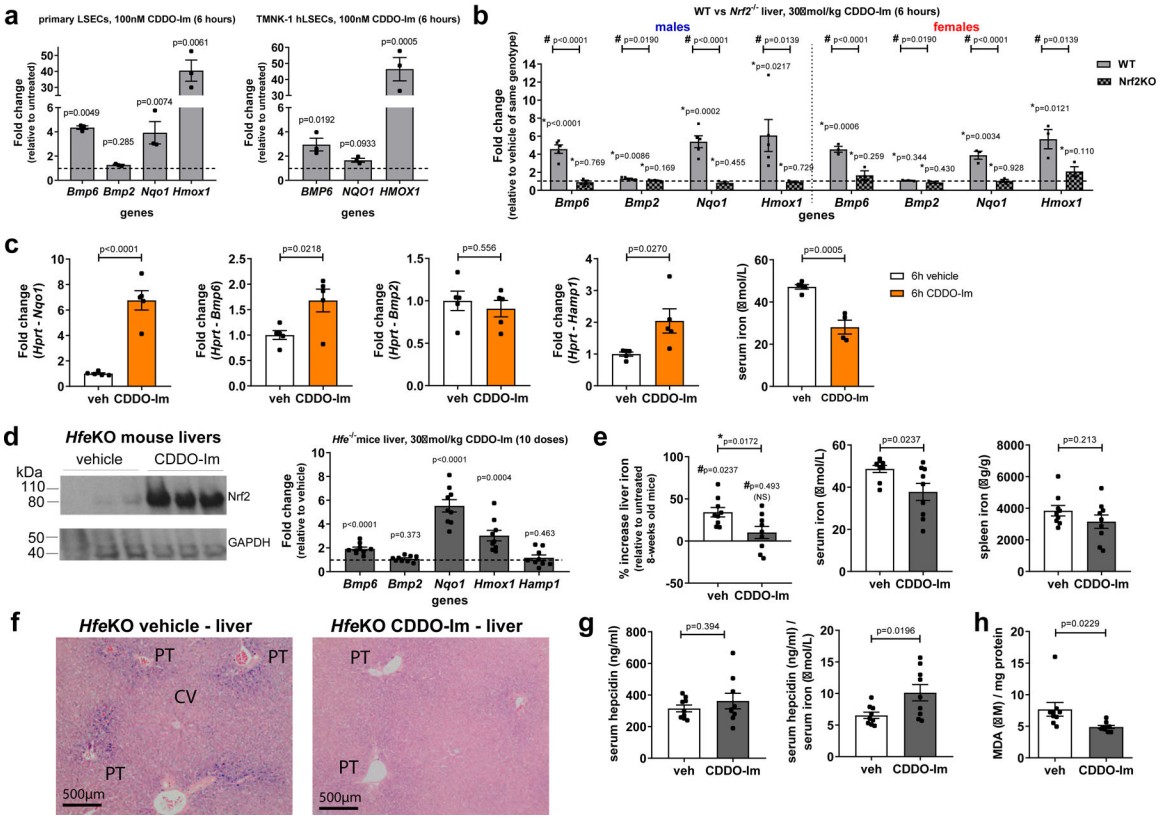

Figure 5.

Small molecule Nrf2 agonist CDDO-Im alleviates iron accumulation in *Hfe*-knockout hemochromatosis mice. **(a)** Primary mouse LSECs and human TMNK-1 cells were treated with 100nM CDDO-Im for 6 hours. Gene expression of *Bmp6*, *Nqo1* and *Hmox1* (and human equivalents) ad *Bmp2*, was quantified by qRT-PCR (n=3 biologically independent samples). **(b)** 6-week old male and female WT and *Nrf2*−/− mice were gavaged with 30µmol/kg CDDO-Im and culled 6 hours post- treatment (n=5 (per group in WT male vehicle or CDDO-Im) and n=3 (*Nrf2*−/− male vehicle or CDDO-Im, WT female vehicle or CDDO-Im, *Nrf2*−/− female vehicle or CDDO-Im) mice). Hepatic gene expression of *Bmp6*, *Bmp2*, *Nqo1* and *Hmox1* was quantified by qRT-PCR. (**c**) *Hfe*-knockout mice were given a single dose of vehicle or 30µmol/kg CDDO-Im by oral gavage (n=5 mice per group) and 6 hours later hepatic expression of *Nqo1, Bmp6, Bmp2* and *Hamp1* was determined and serum iron was quantified. **(d-h)** 8-week old female *Hfe*-knockout mice were given vehicle or 30µmol/kg CDDO-Im by oral gavage for 10 doses over 3 weeks (n=9 mice per group). **(d)** Western blot on liver lysates to detect Nrf2 protein and qRT-PCR to quantify liver gene expression of *Bmp6*, *Bmp2*, *Nqo1*, *Hmox1* and *Hamp1* were performed. **(e)** Liver non-heme iron was quantified and calculated as a percentage of untreated 8-week old female *Hfe*-knockout mice. Serum and spleen iron were also quantified. **(f)** Liver sections from vehicle-treated (left) and CDDO-Im-treated (right) were stained with Perls Prussian blue. **(g)** Serum hepcidin was quantified by ELISA and calculated as a ratio against serum iron. **(h)** Hepatic malondialdehyde (MDA) was quantified by TBARS assay. Statistics for (**a,c,d,e,g,h)**: two-tailed t-test . Statistics for **(b):** Asterisks (*): two-tailed t-test between vehicle and CDDO-Im

groups within same genotype. Hash (#): 2-way ANOVA between wildtype and *Nrf2*-knockout mice given CDDO-Im, stratified by sex. Statistics for left-most graph in **(e)**: Hash: two-tailed t-test between vehicle or CDDO-Im treated mice and untreated 8-week old mice; asterisks (*): two-tailed t-test between vehicle and CDDO-Im group. Data represented with centre values as mean and error bars as SEM.

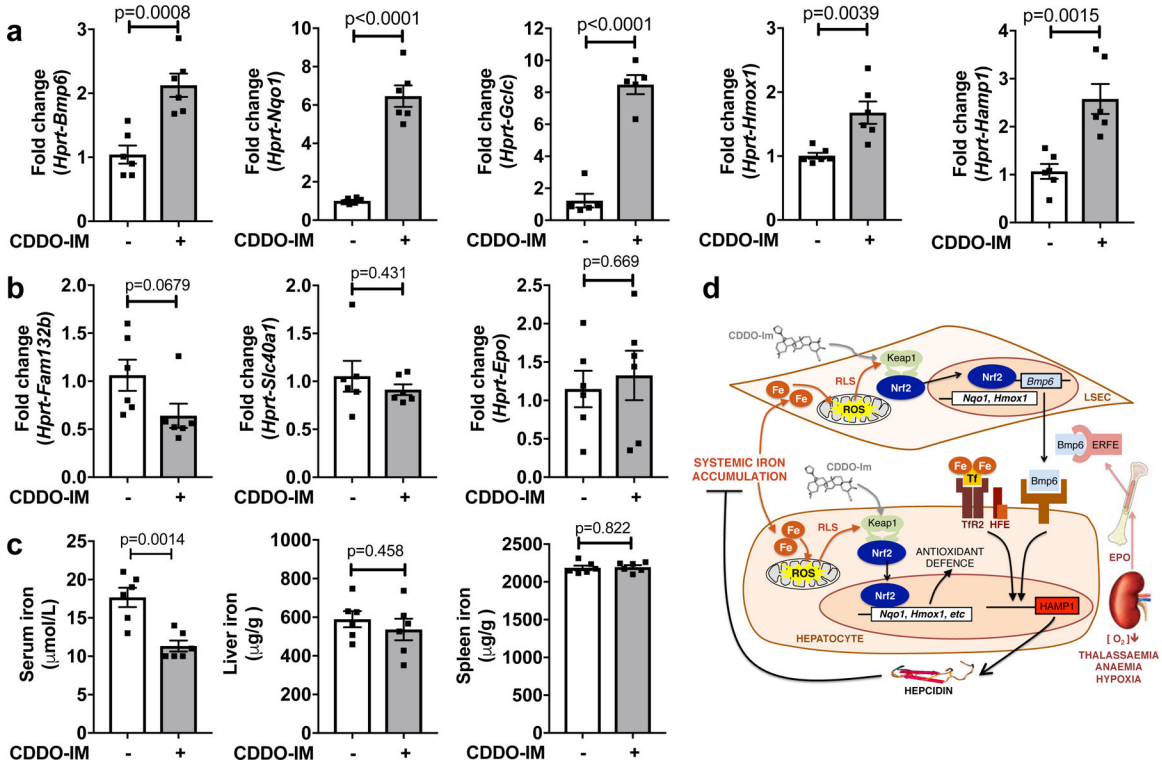

Figure 6.

CDDO-Im alters the Bmp6-erythroferrone axis and decreases serum iron in thalassaemia mice. **(a)** 12–16 week-old male th3/+ mice treated with 100nM CDDO-Im for 6 hours had increased hepatic expression of *Bmp6, Nqo1, Gclc, Hmox1* and *Hamp1.* **(b)** CDDO-Im did not significantly alter splenic expression of *Fam132b* (encoding erythroferrone) or *Slc40a1* (encoding ferroportin) or kidney expression of *Epo.* **(c)** CDDO-Im significantly decreased serum iron but not liver or splenic non-heme iron concentration. (n=6 mice per group for a-c) **(d)** Proposed scheme, depicting activation of Nrf2 in LSECs and hepatocytes by iron-induced mitochondrial ROS and subsequent released RLS, or by CDDO-Im, leading to Keap1 destabilisation, enhanced *Bmp6* (counteracting anaemia-induced erythroferrone) and raised hepcidin, and increased cytoprotection. Two-tailed t-tests were performed between mice treated with vehicle and CDDO-Im. Data represented with centre values as mean and error bars as SEM.